First Monte Carlo studies for the array level trigger system in CTA

Humboldt-Universität zu Berlin
Mathematisch-Naturwissenschaftliche Fakultät I
Institut für Physik

Promotionsvorbereitende Arbeit

vorgelegt von
Manuel Paz Arribas
geboren am 31. August 1983 in Sevilla (Spanien)

Gutachter: Prof. Dr. Thomas Lohse
Prof. Dr. Hermann Kolanoski

Juli 2008

Please refer to this work as
M. Paz Arribas, U. Schwanke, *CTA internal note*, Oct 2008
http://www.cta-observatory.org/ctawpcwiki/images/1/13/CTA_MC_Note1_Trigger.pdf

Contents

List of Figures

List of Tables

Chapter 1

Introduction

The γ ray astronomy has been developed since many years with different kind of experiments: satellites and ground based detectors. The CTA (Cherenkov Telescope Array) project belongs to the latter, in the subclass of IACT (imaging atmospheric Cherenkov telescope) experiments. This kind of experiments consist of ground based telescopes sensitive to the cosmic γ ray spectrum and permit to explore higher energy ranges due to their bigger collection areas.

The field of IACT experiments started with experiments like Whipple and HEGRA (see [1]) and is now very active with experiments like VERITAS MAGIC (see [9]) and HESS (see [25], [24]), and their upgrades.

CTA will be the next generation of IACT experiments.

The aim of CTA is to further investigate the γ ray astronomy in the very high energy (VHE) range from several tens of GeV to 100 TeV with a bigger effective area, a better angular resolution and a sensitivity $\sim$ mCrab flux (10^{-3} Crab Nebula flux), discovering new sources (eventually also new kind of sources) and investigating the origin of the non-thermal cosmic ray emission coming from the space.

At the present time CTA is being designed, so it is not yet sure how the experiment will look like. Nowadays it is likely that it will consist of a $\mathcal{O}(50)$ telescope array with $\mathcal{O}(4)$ big telescopes (diameter $\sim$ 30 m) in the middle and small telescopes (diameter $\sim$ 15 m) ordered around. It is also been suggested a possibility in which the array would have 3 kind of telescopes: big and medium (like in HESS) and some smaller ones dispersed around the array for the high energy events.

For more information see the papers [15], [6] and the CTA web page [10].

The big number of telescopes and the wide covered area will make of CTA the first experiment of its type where the covered area will be significantly bigger than the event Cherenkov lightpool. This represents a new challenge in the sense that all what is being learnt from similar experiments like HESS or MAGIC, or even other kind of particle experiments like Atlas or CMS at LHC can be applied to CTA and also develop new technologies algorithms and strategies. To give an example and being more precise in the topic of this work, it is a new challenge for testing new trigger strategies and develop new algorithms and technologies for it: this work consists of a Monte Carlo study of the trigger for CTA at the inter telescope level. In the second chapter an introduction to the trigger system and a more detailed motivation of this work is presented. In the third chapter the simulation software, the simulated telescope array and the Monte Carlo samples are described. In the fourth chapter the results of the analysis are presented. And in the fifth chapter some conclusions are discussed, together with the following steps concerning the trigger studies.

Chapter 2

Trigger

In this chapter, a description of the trigger system will be presented, together with a more concrete vision of the purpose of this work.

2.1 TRIGGER SYSTEM

The aim of triggering systems on modern physics detectors is to select the events of interest at a rate that can be handled offline. The idea is to keep the event rate as low as possible in order to be able to save the information coming from the detector. The way this is done is to design a more or less complicated system which keeps as much signal as possible and rejects as much noise as possible. This noise could be real background coming from events with similar characteristics as the signal of interest, or some fluctuations due to the electronic signals of the devices and, in the case of γ ray astronomy, also due to night sky background.

As already mentioned, the signal are the γ rays coming from the sources under study: the γ rays have the advantage that they are non charged particles, so the galactic and extragalactic magnetic fields have no influence on them and therefore they can be traced back to the sources where they come from. They also have another advantage in comparison to other neutral particles (e.g. neutrinos) used to do astroparticle physics: they interact electromagnetically, so they have a bigger cross-section and are more easily detected. These γ rays interact with the particles in the atmosphere producing electromagnetic showers (see [25], [24]). The subproducts from the cascade travel at very high velocities (faster as the light in the air) producing Cherenkov light in a cone around the direction of the primary particle. The photomultipliers (PMTs) of the cameras of IACTs are sensitive to this light and record pictures of the events as the Cherenkov light reaches the telescope dish.

For γ ray astronomy, the main background sources are:

- Bright stars: due to the angular resolution of the PMTs ($0.16°$ for HESS) used in the cameras, they produce a hot pixel: a pixel which is constantly above the threshold, so it is turned off.

- Night sky background (NSB): this is a diffuse emission with different sources (diffuse light reflected in the atmosphere, nearby human lights, diffuse scattered star light, ...) that produces randomly triggered pixels, with a signal not coming from the sources under observation.

- Other showers coming mainly from electron and hadron (mainly proton) cascades.

- Cherenkov cones produced by single muons coming from hadron cascades.

In this section we will refer to the three major fonts of noise: NSB, muons and protons.

In order to reduce the rate and try to get rid of the noise and/or background there are some different approaches (topological like in HESS - see [12], [13] - and analog like in MAGIC - see [8]), but essentially with the same steps:

Level 0 ($L0$): a pixel threshold.

Level 1 ($L1$): a timing and spatial coincidence of pixels.

Central trigger (CT): a coincidence trigger between telescopes (if the is more than one) within a certain time window.

2.1.1 Night sky background

As already said, NSB produces randomly distributed triggered pixels. By selecting an appropriate pixel threshold, most NSB can be rejected, in order to have a very small probability of a $L1$ trigger.

2.1.2 Muons

Muons produce a Cherenkov light cone very low in the atmosphere, so they produce a small ring-form lightpool at ground and therefore are only seen by single telescopes, so a request of multiplicity of telescopes (if possible) avoids triggering such events.

This is not possible in case of monoscopy, and the cut should be applied after the parametrization of the pictures (see [24]).

2.1.3 Hadronic background

Hadrons are the main component of the cosmic rays, and hence produce the biggest trigger rate. Most of the hadrons are protons, and the heavier elements, such as helium, are very rare compared to protons. For this reason, in this work, only protons are taken into account to estimate the background.

Protons produce hadronic cascades very similar to the electromagnetic ones produced by γ rays. For this reason, it is very complicated to distinguish between them at the trigger level and the separation is done offline (see [3] for different background models). As they are the main component of the cosmic radiation, they dominate the trigger rate, and one can say that the total trigger rate of the system is due to protons.

2.2 TRIGGER AND CTA

It is not yet clear which approach will have the trigger for CTA (digital or analog). What is sure is that it will be more complicated than the trigger from the previous experiments (HESS and MAGIC). In this work, a certain $L1$ is assumed, and higher inter-telescope trigger levels are investigated in a first approach. In the end, if the rate is too high, a scaling method can be applied, where events are randomly rejected in order to reduce the rate.

2.2.1 Trigger studies

The purpose of this work is to make a first study of the telescope level trigger for CTA. For this purpose, on the base of HESS, the software is being adapted and developed in order to be able to study the trigger of IACT arrays like CTA under different aspects:

- What trigger rate is expected?
- How many telescopes should be read out?
- How big will be the data transfer?/It is possible to reduce it?

The latter covers the other two, but also depends on what information will be saved per event (e.g. if timing information will be saved or not). It is primary to develop an intelligent trigger strategy that allows to reduce the trigger rate of the telescope in order to have an affordable data rate which can be processed.

This work is the first study of the trigger at the telescope level, so the results coming in the next sections are not to be taken as definitive: the array aspect will change and some new strategies and studies will come.

Chapter 3

Description of the simulation

This chapter consists of a description of the software used, the telescope array and the Monte Carlo data.

3.1 SIMULATION SOFTWARE

The software chain used for the analysis of the MC data is one of the possible software chains used as a standard in the HESS collaboration. It should be said, that this software is being modified in order to be able to use it for CTA. And a part of it will be made public for this purpose.

It should also be mentioned that the whole software has not yet be modified, so only a reduced part of it is used. That leads to some simplifications in the analysis chain: as there is still no specific configuration and/or cuts for the CTA data, no shower reconstruction is possible, and the histograms presented are functions of the parameter of the true shower (the parameter used in the simulation). But still, this does not affect to the results presented here, since we are studying the performance of the system at the trigger level.

The software chain consists basically of three steps: shower generation, detector simulation and analysis. Each of these steps is explained in more detail in the following.

3.1.1 Shower simulation: CORSIKA

This is the software package used for the shower simulation in the atmosphere. First of all the cascade is generated starting from a primary particle (in this case a γ-photon or a proton). Then, the interaction with the atmosphere is simulated. And in the end, only the Cherenkov photons which will hit the detectors (roughly simulated by spheres) are kept and passed to the detector simulation.

For more details see [5].

3.1.2 Detector simulation: sim_hessarray

This is the software package used for the detector simulation. It is the specific modification of sim_telarray which has been done for the HESS system. It takes the results coming from CORSIKA and simulates the reflection of the Cherenkov light in the telescope mirrors and its detection on the cameras.

During the detector simulation, NSB is simulated, but only when a particle hits a telescope, so one has to extra calculate the rate due to random NSB coincidences afterwards and add it to the calculated rate from the simulations. It is also important, that no time window for the telescope coincidence was simulated, so one can calculate this rate for whatever time interval.

The result of this simulation is a raw data file with equivalent information as a normal run file of real data taken with the HESS system.

In this step, a trigger criterion is applied to the data, and only the events passing this criterion are saved to disk (like the real data).

For more details see [5].

3.1.3 Analysis software: SASH and HAP

The files are converted to a more appropriate format called SASH (Storage and Analysis Software at HESS) which essentially is a root format with special classes developed for HESS.

Then, the raw Monte Carlo files are converted to DST format, in order to be processed by the HESS software using the new developed framework HAP (HESS Analysis Program).

The main difference between raw and DST files is that in the latter, image cleaning has been done, so they are much more reduced files which also are faster to analyze.

For more details see [16], [26], [17] for SASH and [18],[19] for HAP.

3.2 SIMULATED DATA

In this section a more detailed overview of the telescope system and the used data sets is presented.

3.2.1 Telescope array

The simulated array consists of a squared symmetry 97 telescope array with 12 big (HESS 2 like) telescopes in the middle and 85 small ones (HESS 1 like) distributed gradually in a 1 Km^2 area (see figure 3.1 for the layout of the array).

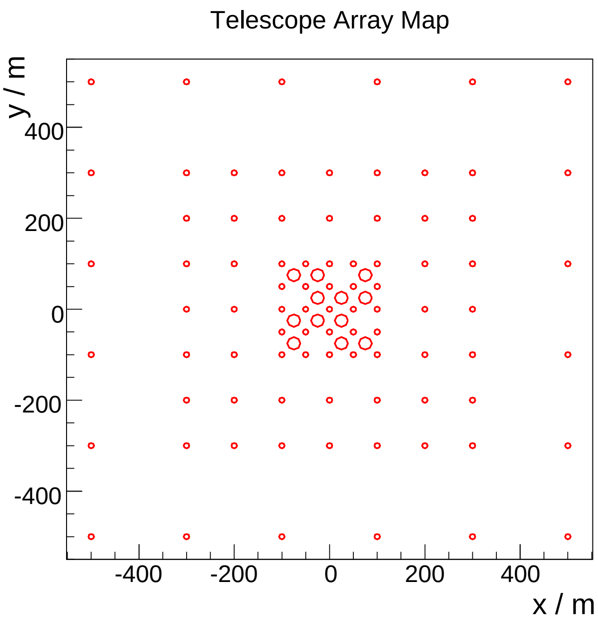

Figure 3.1: Layout of the telescope array at the ground: each circle represents a telescope. The sizes of the telescope dishes are indicated by the different radii of the circles.

The telescopes are not uniformly distributed, but gradually, so that there is a bigger density in the center (for the detection of low energy events: small Cherenkov lightpool and less Cherenkov light) and small density but covering a big area in the outer part (for the detection of high energy events: greater lightpool with more light, but more rare according to the spectral power law).

The main features of the array are listed in the following table, where the properties are referred to both telescope types: first the big ones, then the small ones (see also [4]):

- Altitude: 1800 m
- Atmosphere: Windhoek Namibia all year average
- 97 tels: 12 big (HESS 2 like) 85 small (HESS 1 like)
- Radii: 16.00 m, 7.50 m
- Focal length: 35.10 m, 15.00 m
- Camera pixels: 4093, 1735
- Pixel size: 3.9 cm

- Field of view (FOV) diameter: 5°, 7°

In figure 3.2 there is an image of the positions (x and y coordinates) of the photomultipliers (PMTs) of the camera on the camera focal plane, superimposed for both sizes of cameras for big and small telescopes.

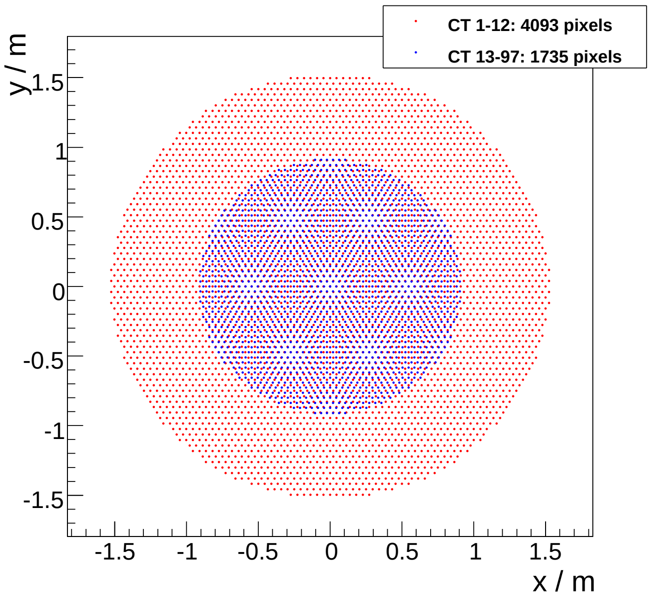

Figure 3.2: Position of the PMTs of the cameras in the camera focal plane: the configurations for the 2 kind of cameras are superimposed to show the different sizes. The big cameras (CT 1-12) have a 5° diameter FOV, and the small ones (CT 13-97) a 7° diameter FOV. "CT" means Cherenkov telescope.

3.2.2 Simulated trigger criterion

As already mentioned in section 2.1, the trigger consists of two parts. The conditions applied to the data analyzed in this work were:

- $L1$: 3 pix $>$ 4 p.e. (SmartPixel): 3 next-neighbouring pixels must have a signal of at least 4 photo-electrons for the level 1 trigger.
- Central Trigger: at least 2 telescopes of the whole array must have a $L1$ trigger. That would reject all the monoscopic events, which have a more complicated reconstruction, and thus have a bigger error.

In the simulation the pixel threshold is adjusted in order to have a telescope random trigger rate due to NSB smaller than 100 Hz.

The difference between the approaches of MAGIC and HESS (analog vs. digital) comes in the $L1$ trigger: the topological trigger from HESS requires a certain pattern in the camera (for HESS the camera was divided in overlapping sectors of 64 pixels and the requirement was that 3 pixels in a sector above 4 photo-electrons produces a $L1$ trigger), whereas the analog system from MAGIC studies the time evolution of the pixel signal to produce a trigger.

Actually, for the CTA simulations, a different concept for $L1$ was used: the SmartPixel: each pixel knows its next neighbours (see figure 3.3), so the triggered signal is compact (the expected pattern of a γ ray is a compact ellipse-like image in the camera).

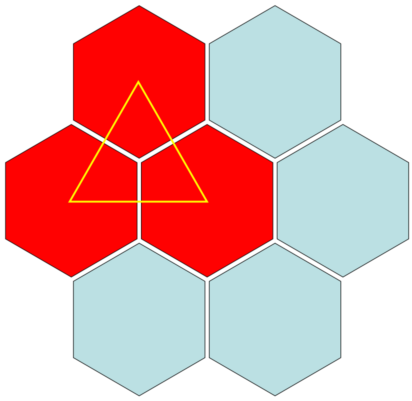

Figure 3.3: SmartPixel: each pixel is connected to its next neighbours, so that compact images are triggered. In the picture, the blue hexagons represent pixels below the threshold and the red ones pixels above the threshold. The yellow triangle is drawn to emphasize the telescope trigger condition: 3 next-to-each-other pixels above 4 p.e.

3.2.3 MC samples

In this subsection the Monte Carlo data used for the analysis is presented.

Two sets of different simulated particles were analyzed: γ rays to get an idea of the efficiency of the detection of sources, and protons to estimate the background.

The files have been produced with the chain described in the software section. And consists of two samples of γ rays and protons simulated at a zenith angle of 20° and azimuth 180° (south).

The simulation radius around the pointing direction of the array is 1500 m for the γ rays and 2000 m for the protons.

In addition, for the γ rays a wobble offset of 0.5° between direction of the simulated γ ray point source and the camera center was taken. For the protons, a diffuse emission has been simulated: the direction of the primary particle is not always the same as for point sources, but are generated within a cone of angular radius 7° around the pointing direction of each telescope.

The main properties for both sets are summarized in the following list:

- γ rays (20° zenith south, 0.5° offset)
  - Energy range: 5 GeV to 10 TeV
  - Spectral index: -2.0
  - Simulated events: 1.78×10^7
  - Read events (2tels): 400000
  - Data equivalent to 3.24 Crab Nebula hours data taking.
  - Simulated NSB: 100 MHz p.e. / channel
- Protons (20° zenith south)
  - Energy range: 10 GeV to 20 TeV
  - Spectral index: -2.0
  - Simulated events: 1.22×10^8
  - Read events (2tels): 298891
  - Data equivalent to 7.47 BESS spectrum seconds data taking.
  - Simulated NSB: 100 MHz p.e. / channel

In the list, "read events" are the events selected by the trigger criterion from the simulation programs described in 3.1.2.

For comparison for the times, a normal run for HESS takes 28 min.

The simulated NSB depends on the pixel angular resolution and on the PMT quantum efficiency [1].

[1]The simulated NSB was too low: due to the high quantum efficiency of the PMTs, the simulated NSB rate should have been 50% higher than what it was measured, so the pixel threshold should also be higher.

Chapter 4

Results

In this chapter a description of the analysis procedure is presented, together with the results and a first look into them.

4.1 TRIGGER CRITERIA

The Monte Carlo files were produced by Konrad Bernlöhr in Heidelberg with the simulated trigger decision described in the subsection 3.1.2.

On the base of these simulations, the files are converted to SASH DST format and then processed in the software chain from HESS with HAP. γ rays and protons are analyzed separately in the chain, where more complicated central trigger decisions are simulated. In table 4.1 there is a description of the different trigger criteria which were simulated for this analysis. There is as well a reference to the color pattern each trigger criterion will be represented with in the following figures.

Trigger criterion	color	Description
2tels	black	at least 2 tels out of 97 (stereo events)
bigtels	red	stereo events, but at least one tel must be big
neighbours	green	stereo events, but at least 2 tels must be neighbours
reduced_array	blue	same as neighbours, but with less telescopes

Table 4.1: Simulated trigger criteria at the telescope level. The colors are used to refer to each trigger criteria in some of the following plots.

Looking into more detail to the trigger criteria,

2tels takes all the stereoscopic events. This criterion basically takes all the events which are in the Monte Carlo files, since it is the same criterion they were created with. This is the starting point and hence it is expected to have the biggest trigger rate in the end.

bigtels requires at least one big HESS 2 like telescope (CT 1 to 12), so it can be taken as a measure of the rate due to the big telescopes. As those telescopes have a bigger collection area, and hence are able to detect events at lower energies (the most frequent ones due to the spectral energy dependence - see figure 4.10), the trigger rate is expected to be high.

neighbours employs a more intelligent use of the array, where each telescopes is connected to all of its next neighbours, so one can really trigger on stereo events, and get rid of events where two (or more) far from each other telescopes have triggered (random NSB triggering). In figure 4.1 (left) one can see the connections between the telescopes. This can represent a difference in the trigger system, where instead of a big central trigger box responsible for all the telescopes, a decentralized system can be chosen with a smaller trigger box for each group of neighbouring telescopes (see [14]).

reduced_array is like "neighbours" but with a reduced array: as the 97 telescope array is likely too big for the actual CTA budget, one can try to leave out telescopes. In this case the outer layer of big and small telescopes respectively are ignored, so the array would look like in figure 4.1 (right). This array with 69 telescopes might still not be doable, but at least it could be more realistic, from the number of telescopes point of view.

4.2 TRIGGERED DATA

After processing the files for each trigger criteria, one can look into more detail to the events triggered by each criterion.

4.2.1 Shower core

The shower core is the point where the primary particle would have hit the ground if it would not have undergo in interactions with the atmosphere particles (and hence produce a cascade).

It is interesting to look at where do the events trigger. From that, one can see how efficient is the array and infer how far away should the telescopes be, in order to cover the maximum possible area (interesting for high energy events, which have a bigger lightpool, but are more rare) without loosing too many events in between.

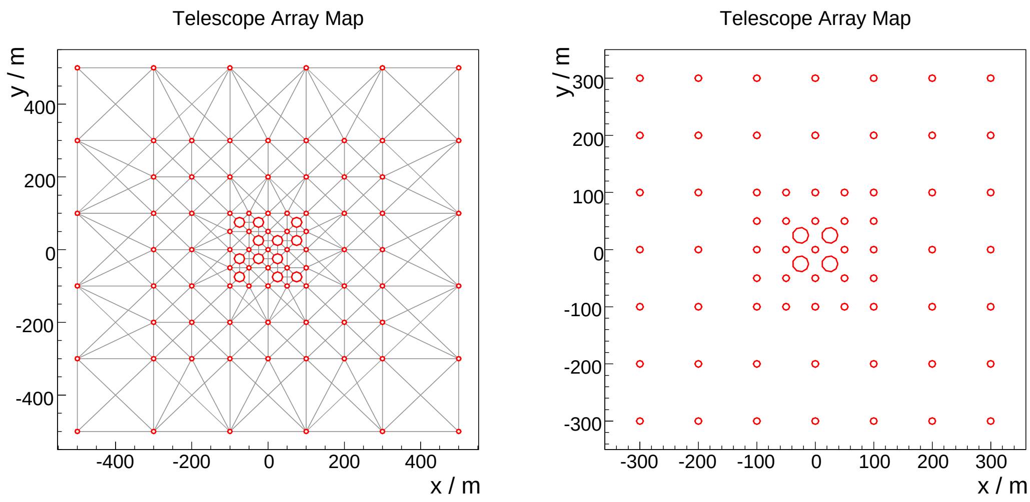

Figure 4.1: Left: telescope array with the connections between telescopes. The big telescope cells are interconnected (also when a small telescope is in between). Right: reduced telescope array (69 telescopes): the outer layers of big and small telescopes respectively have disappeared. Notice that the area covered by the array is smaller: 0.36 km^2. The telescopes are also connected in a similar way like in the left picture.

For this purpose, the map of the shower core position (x and y coordinates) of each triggered event is presented for each trigger criterion in figures 4.2 for γ rays and 4.3 for protons.

To produce these maps, the events have been weighted, in order to represent a more realistic spectra in each case: a 2.39 index power-law for the γ rays, and a 2.70 index one for the protons (see subsection 4.3.1). It is also worth to mention, that the coordinate system used for this plot is the same one as for figures 3.1, 4.1 and 4.1 for the telescope arrays.

The general trend in the pictures is a big density of triggered events in the center which decreases towards the edges. There are more events in the center because of the bigger density of telescopes and also due to the big telescopes, which are expected to be triggering at a higher rate than the small ones. And since the layout of the big telescopes is more round than for the small ones, one can see that this bigger density of events in the center are more round-like distributed.

Comparing both sets of pictures, one can see that the proton events are more spread than the γ ray ones, which are more localized in the center of the picture (where the telescope array is localized). Moreover, the distribution of the events for the γ rays is more squared, representing the squared symmetry of the array, whereas the protons are more round (reaching the maximum distance within

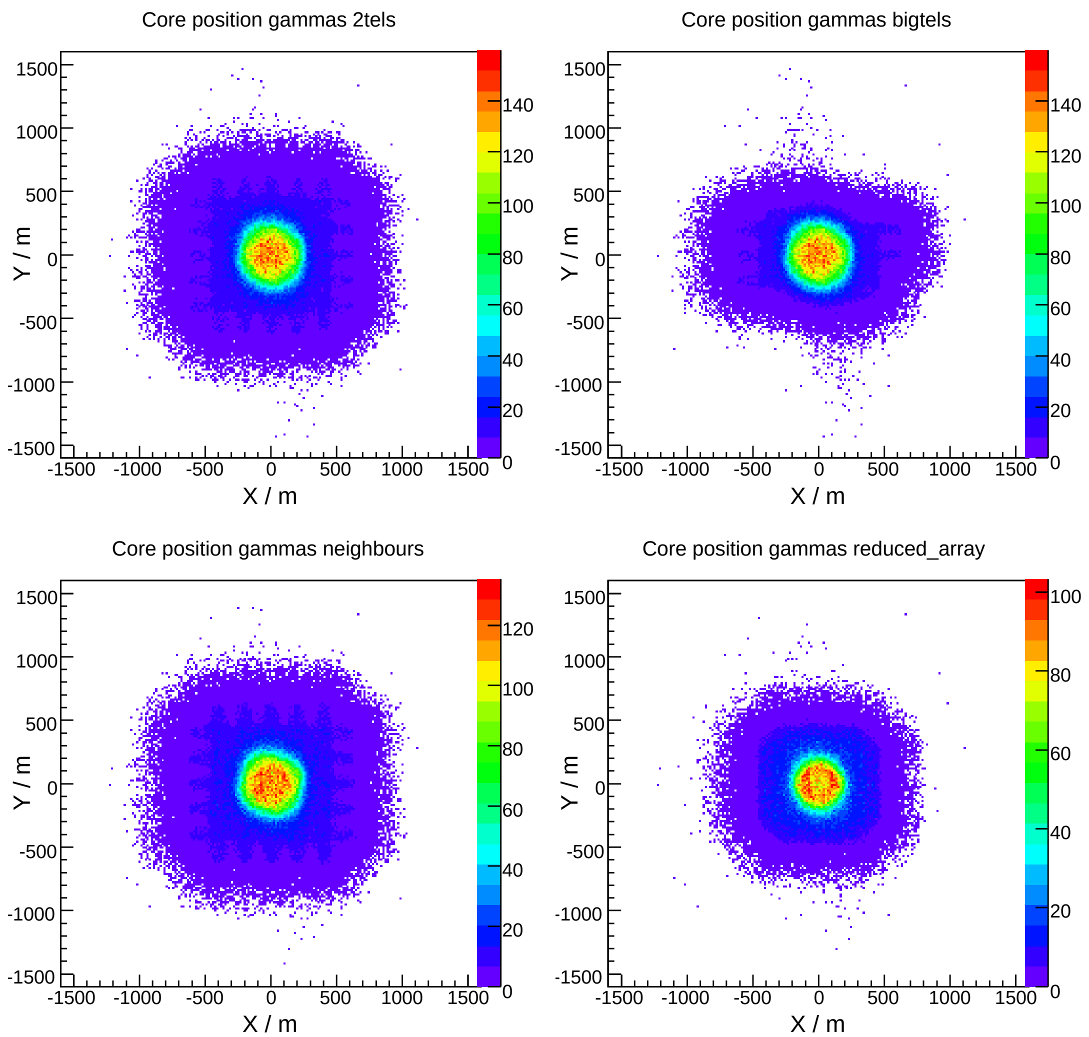

Figure 4.2: Core position at ground for γ rays: hypothetical impact point of the primary γ ray if it would not have interacted in the atmosphere producing a shower. The represented value is the real value used for the Monte Carlo simulations. The events have been weighted in order to represent a 2.39 index power-law. There is a plot for each of the trigger criteria described in table 4.1.

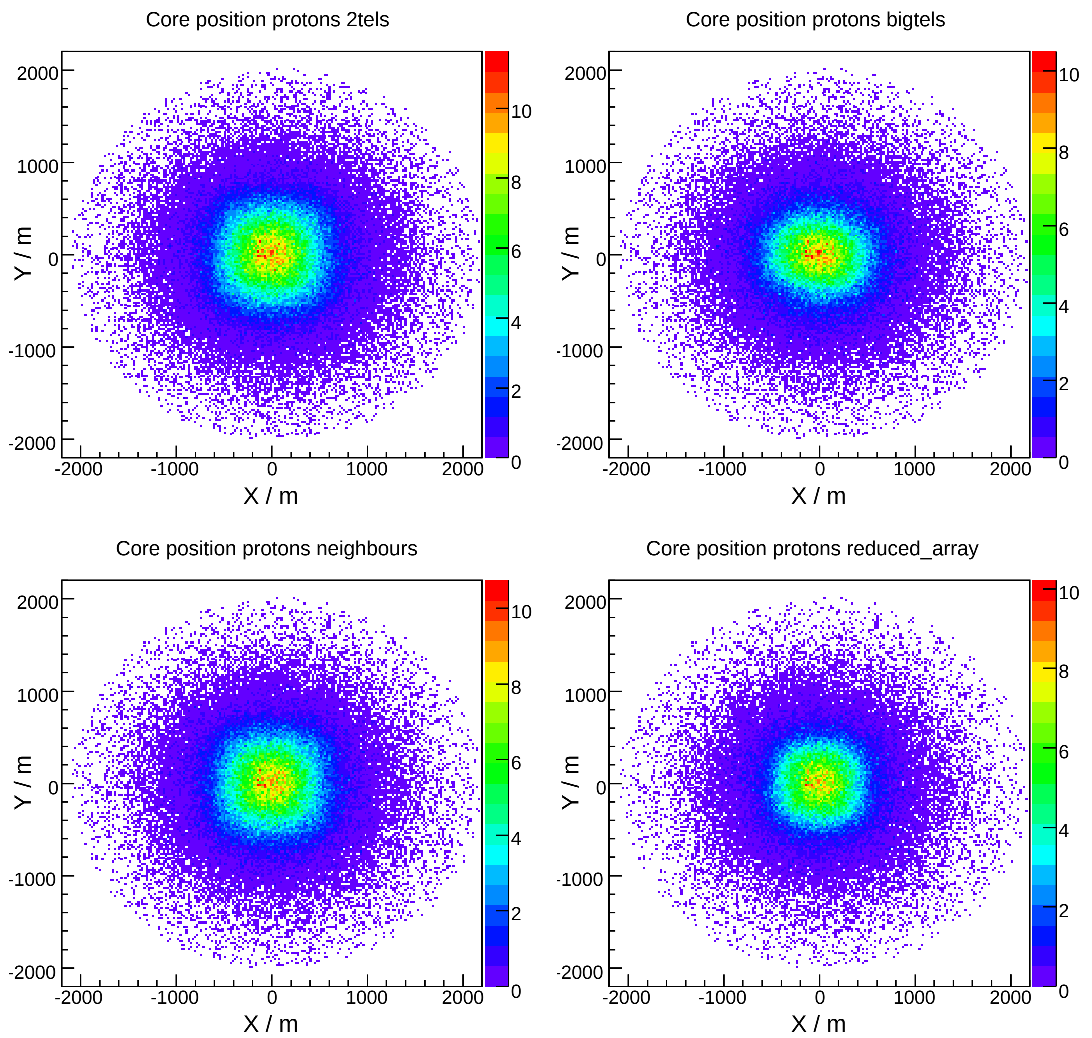

Figure 4.3: Core position at ground for protons: hypothetical impact point of the primary proton if it would not have interacted in the atmosphere producing a shower. The represented value is the real value used for the Monte Carlo simulations. The events have been weighted in order to represent a 2.70 index power-law. There is a plot for each of the trigger criteria described in table 4.1.

showers are simulated (see 3.2.3). The reason for that, is that the proton showers are more spread (and also more irregular), so more far away events are triggered.

Among the different trigger criteria, there is not a big difference in the proton distribution, except for a more elliptical distribution along the North-South direction (parallel to the x axis of the figure). This anisotropy is also present at the γ ray distribution, showing that the telescopes are pointed towards the South. Among the γ ray figures, the differences are more clear: for the neighbouring scheme (top left) and the one triggering all stereoscopic events (bottom right) the distribution covers exactly the 1 km^2 surface of the array. For the reduced array the result is similar, but for a smaller surface, and for the big telescopes scheme, the pattern is elliptical, as already described, and hence does not profit of the whole extension of the array.

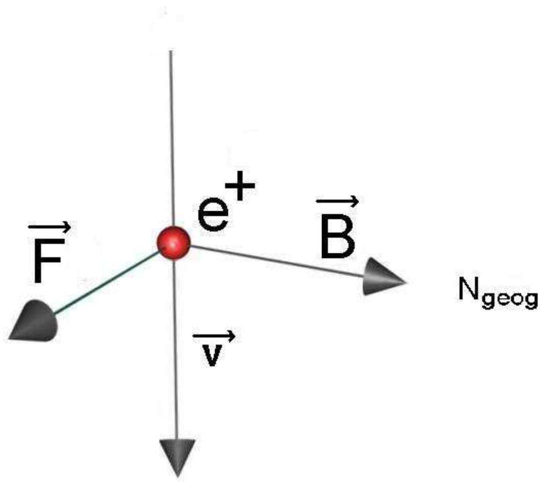

Figure 4.4: Lorenz force acting on a positron coming from a shower cascade.

There is also an interesting asymmetry in the γ ray maps in form of spread events in a quasi-vertical line at $x = 0$ m. These are far away events since what is represented is the simulated shower core and not the reconstructed one. Knowing that the Geographical North of the Earth is in the direction of growing x, then these events are more or less distributed in the East-West direction. One possible explanation for this asymmetry could be that these events come from primary particles with a very low energy. Assuming that, the subparticles of the cascade would also have low energies, especially the charged ones (electrons and positrons), and hence are more susceptible of deflection due to the Earth's magnetic field. As its field lines at the Earth surface go from South to North, the charged particles flying from above-down are deflected in the East-West direction (see the schematic of figure 4.4). That would produce that the far away low energy events along the East-West axis of the array would trigger the central big telescopes and hence would be detected. One should expect that such events will have a very poor reconstruction and therefore, they would be rejected by the cut selection.

This behaviour was already seen in Monte Carlo simulations done for HESS Phase 2 (see [20] [11]).

4.2.2 Triggered telescopes

It is also interesting to see how many telescopes trigger each trigger scheme and how far they are from each other. On the one hand, from this information one could infer how far away should the events be read (how many telescopes should be read per event and how big should the trigger window be) and on the other hand, the number of triggered telescopes is needed to calculate how much disk space per event will be needed.

To see the energy dependence, the plots in this subsection are also done for different energy ranges. Those are described in table 4.2.

event type	color	energy range
all events	black	5 GeV $< E_\gamma <$ 10 TeV; 10 GeV $< E_\mathrm{p} <$ 20 TeV
low energy	light green	$E <$ 100 GeV
medium energy	dark yellow	100 GeV $< E <$ 1 TeV
high energy	light red	$E >$ 1 TeV

Table 4.2: Defined energy ranges and color codes for some of the following plots. Notice that γ rays and protons have different energy ranges.

It is worth to mention that the incoming results for the different energy ranges are not to be compared directly between γ rays and protons. There are two reasons for this:

1. The energy ranges are not exactly the same for both kind of particles as shown in table 4.2.

2. The telescope system is not equally sensitive to both γ rays and protons. As it will be explained in subsection 4.3.4, protons are detected with 1/3 of their energy: for equal primary energies, protons leave approximately 2/3 less Cherenkov light than γ rays in the telescopes.

For those reasons, only the results for the whole energy range are quite comparable: 5 GeV - 10 TeV for γ rays, and 3 GeV - 6 TeV for protons as they are seen by the telescopes.

Having said this, the distributions of the number of triggered telescopes is shown in figures 4.5 for γ rays and 4.6 for protons. There is one plot for each trigger criteria, where 4 curves are shown for the different energy ranges specified in table 4.2. The events have been weighted to represent a more realistic spectra in each case: a 2.39 index power-law for the γ rays, and a 2.70 index one for the protons (see subsection 4.3.1).

The general trend for each curve is a peak with a steep decrease at low number of telescopes, which becomes more flat at medium number of telescopes and a steep fall to zero towards the end. Eventually, there is a plateau at the middle of the distribution and a broad peak before the final fall to zero (to be seen at the high energy curves for the γ ray case). All histograms start abruptly at 2 telescopes because of the trigger condition.

Actually the expectation, for each energy, would be a certain distribution (more or less Poisson like) around a mean value, due to statistical fluctuations. The fact that the plots are not shown for a certain energy but a range of energies modulated by a certain spectrum (see figure 4.10) makes the plots decrease more or less exponentially after the mean value. The peak at low number of telescopes is due to the finite size of the array: the events triggering at the border are detected, but the lightpool does not totally overlap with the telescope array, so they are only seen by a smaller part of the array.

Looking at the different energy ranges, the contribution to the overall (black) curve at low number of telescopes is dominated by low energy events (green curve), at medium number of telescopes is dominated by medium energy events (yellow curve) and at high number of telescopes the high energy events (red curve) dominate. This is not exactly the case for the proton distributions because the low energy range is smaller and hence both, low and medium energy events, have strong contributions at low number of telescopes. These variations with the energy are explained by the fact that both, the size and the photon density of the shower lightpool at a certain height (at the ground in this case), increase with the energy of the primary particle, so low energy showers trigger less telescopes than high energy ones. There are even some high energy events which trigger almost the whole array (91 telescopes).

The major differences between the proton and γ ray curves is the steeper fall of the proton curves towards high number of telescopes. This effect is explained by the different energy spectrum indexes used for the weighting of the events.

Comparing the different trigger criteria, all perform quite similar, except for the reduced array, where the effect of the smaller array makes the curves fall faster, with an abrupt cut at 69 telescopes: at this point, all the telescopes from the array are triggered.

To better compare the different trigger criteria it is also possible to take the mean value for each energy range and plot it as a function of the energy for all the schemes together (left side of figure 4.9).

The tendency is that more telescopes are triggered when the energies increase,

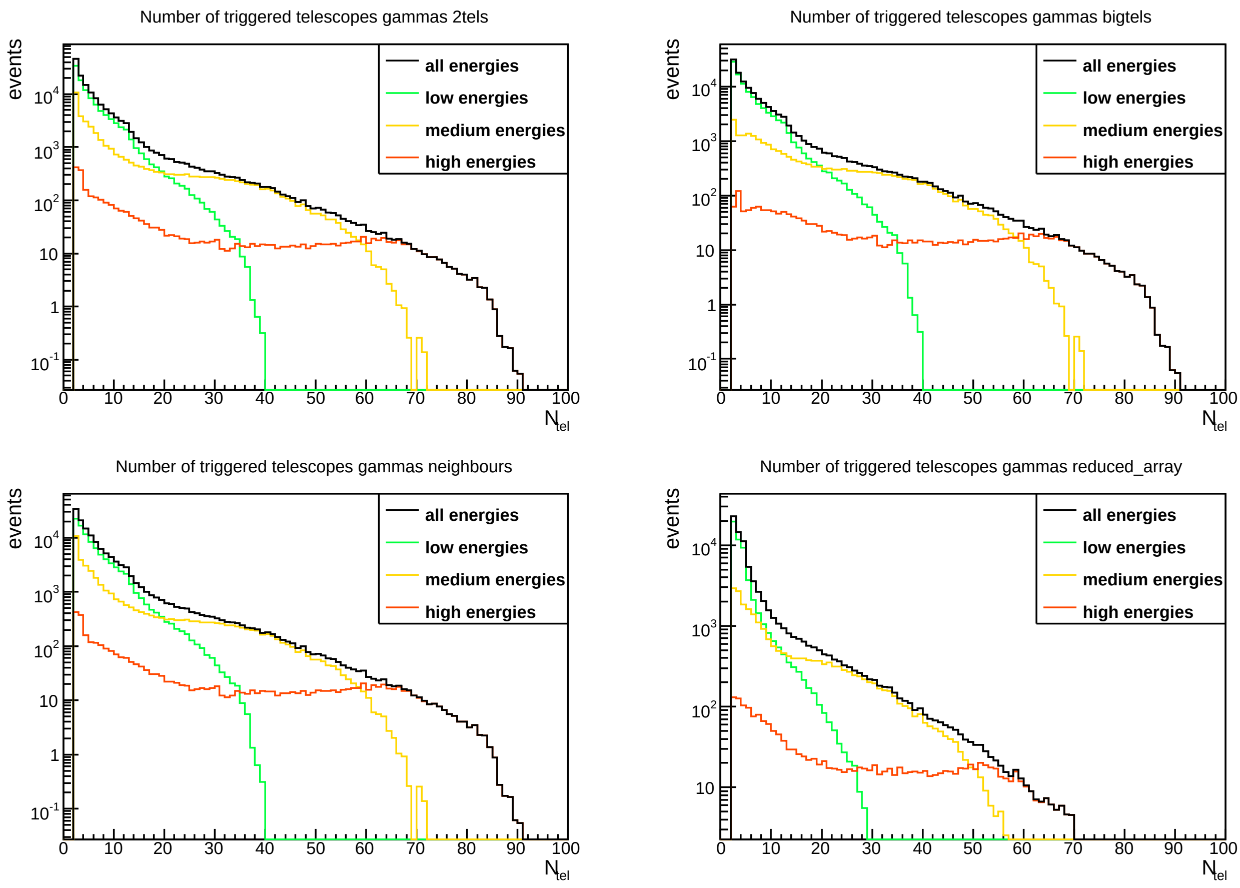

Figure 4.5: Distribution of the number of triggered telescopes for γ rays. The different colors represent different energy ranges (see table 4.2). The events have been weighted in order to represent a 2.39 index power-law. There is a plot for each of the trigger criteria described in table 4.1.

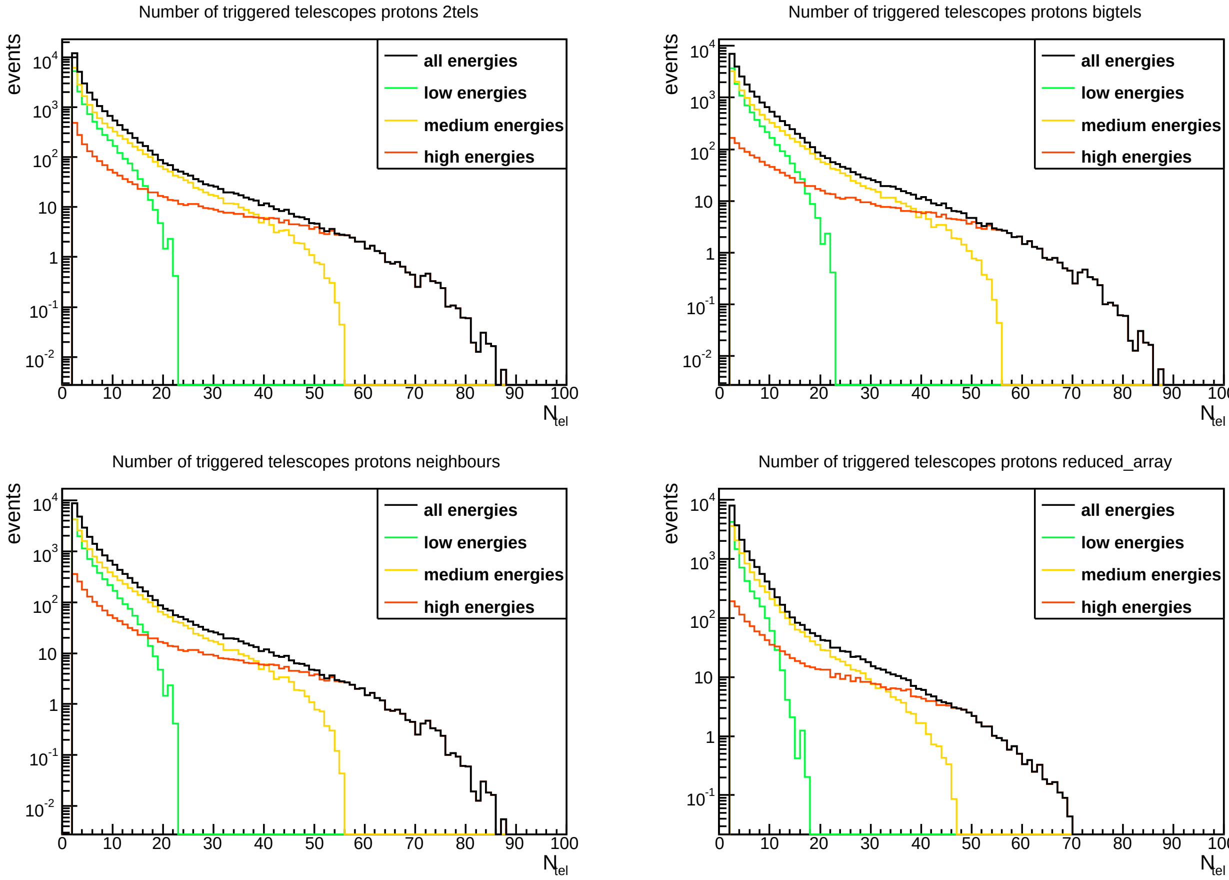

Figure 4.6: Distribution of the number of triggered telescopes for protons. The different colors represent different energy ranges (see table 4.2). The events have been weighted in order to represent a 2.70 index power-law. There is a plot for each of the trigger criteria described in table 4.1.

as seen in figures 4.5, 4.6. At low energies all trigger criteria perform in a similar way, only at higher energies the big telescopes make a difference (red points): the big telescopes tend to trigger events which are more centered in the array, so the contribution is double:

- The array is more dense in the middle.
- The border effect is minimized, because the area where big telescopes are is surrounded by small telescopes.

In any case, the number of telescopes would be bigger.

The contribution of a more dense array is also seen in the blue curve (reduced array), which is also bigger than the green (neighbouring telescopes) and the black one (all stereoscopic events) - the latter 2 performing very similar to each other.

The differences are smaller in the case of protons, due to their bigger and more irregular lightpools.

Switching to how big an event can be (how big its lightpool is), in figures 4.7 and 4.8 one can see the distribution of the maximum distance between pairs of triggered telescopes scaled to the size of the characteristic array cell - 50 m - which is the smallest distance between neighbouring telescopes of the same size (e.g. the 4 big telescope cell in the center of the array): the size of the other possible squared cells parallel to this one, is a multiple integer of the size of this one unitary cell. This value will be referred as distance parameter. The figures are done for γ rays and protons respectively.

In these plots one can see more or less the same trend like in figures 4.5 and 4.6. Each histogram is distributed around a most probable value (peak), which is bigger for bigger energies. The explanation is related to the number of triggered telescopes: the bigger the energy is, the more telescopes trigger, and hence, the more unitary cells of the array are triggered, so the peak of the distance parameter histograms moves to bigger values as the energy increases.

There are some “holes” in the distributions because of the inhomogeneities in the telescope array: the existence of big and small telescopes and the increasing separation between next-neighbouring telescopes as the telescopes are further away from the center of the array (see figure 3.1). Those effects can produce that some distance parameter values becomes less probable than others.

Comparing the γ ray and proton plots, the contributions of the curves at low distance parameters are more important for the at the proton case. This is produced by the fact that proton showers are more spread, so their showers can be detected at a higher distance as seen in figure 4.3, having a bigger probability of triggering the outer layers of the telescope array, where the telescope density is lower, and hence, having a bigger chance of triggering less telescopes. This effect can also be seen for the number of triggered telescopes in figure 4.6.

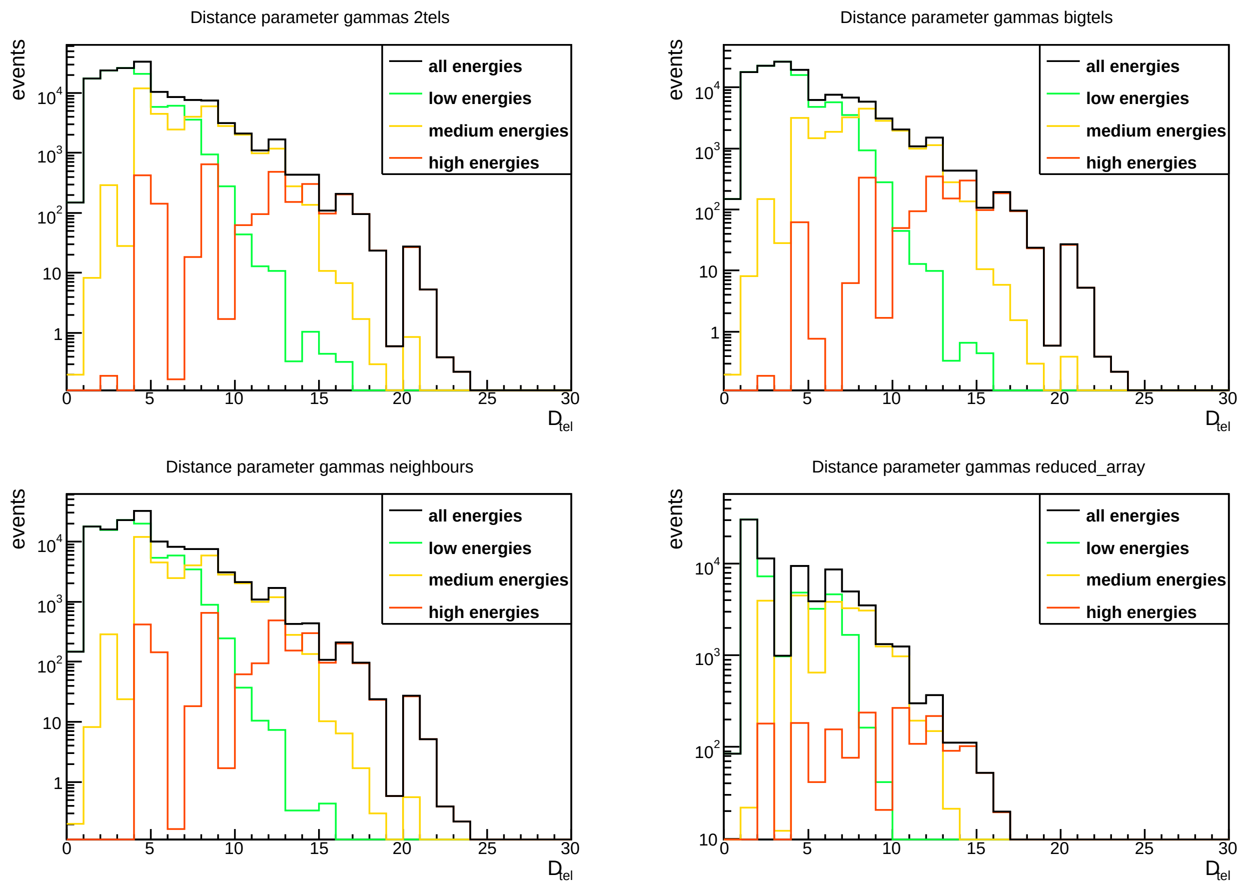

Figure 4.7: Distance parameter for γ rays: distributions of the maximum distance between triggered telescopes scaled to the characteristic distance of the array - 50 m - for each trigger criterion. The value of 20 corresponds to the length of the side of the array (1 km). The different colors represent different energy ranges (see table 4.2). The events have been weighted in order to represent a 2.39 index power-law. There is a plot for each of the trigger criteria described in table 4.1.

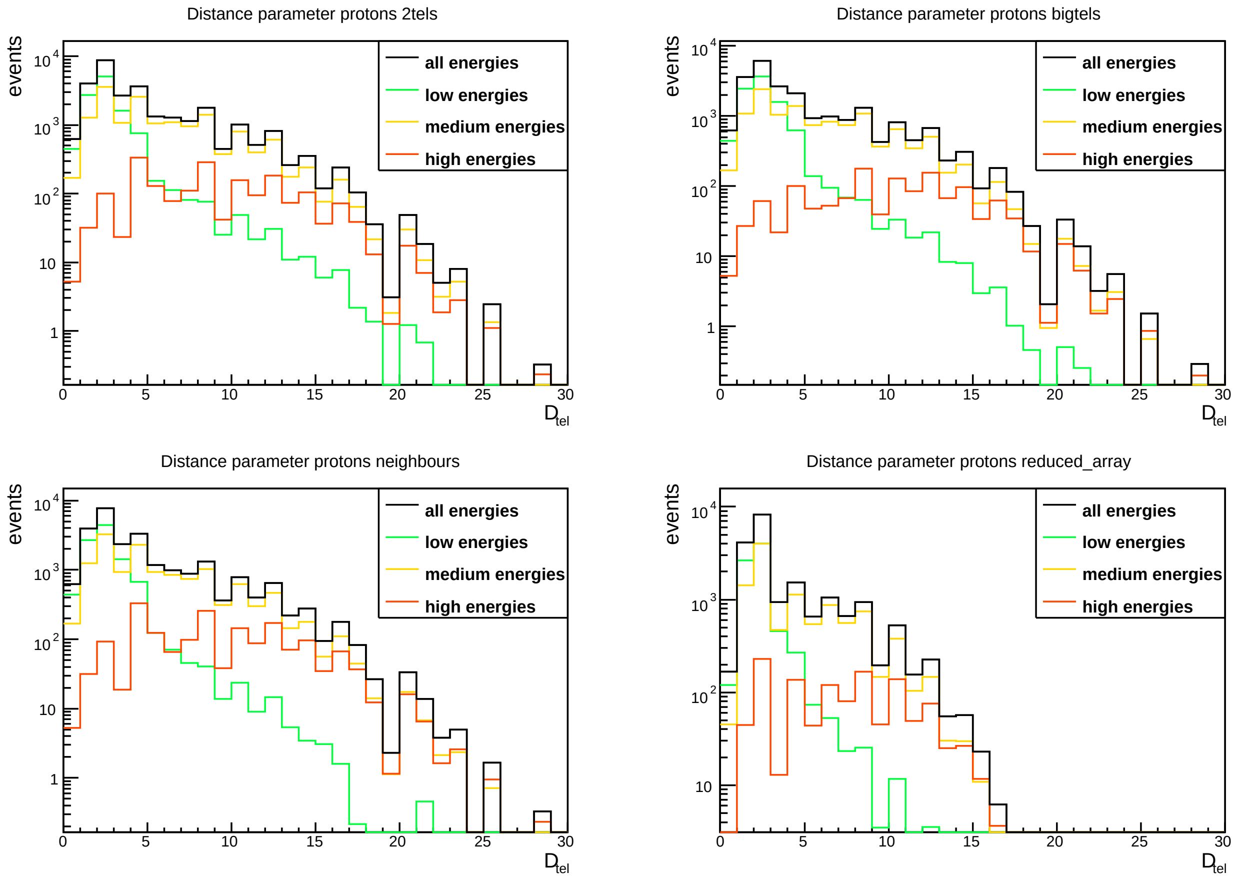

Figure 4.8: Distance parameter for protons: distributions of the maximum distance between triggered telescopes scaled to the characteristic distance of the array - 50 m - for each trigger criterion. The value of 20 corresponds to the length of the side of the array (1 km). The different colors represent different energy ranges (see table 4.2). The events have been weighted in order to represent a 2.70 index power-law. There is a plot for each of the trigger criteria described in table 4.1.

Looking at each trigger criteria, the distributions look quite similar among them. Only the ones corresponding to the reduced array fall to zero at lower distance parameters than for the other criteria, due to the lower extension of the array. However, it is easier to appreciate the differences looking at the mean values for each energy band (right part of figure 4.9).

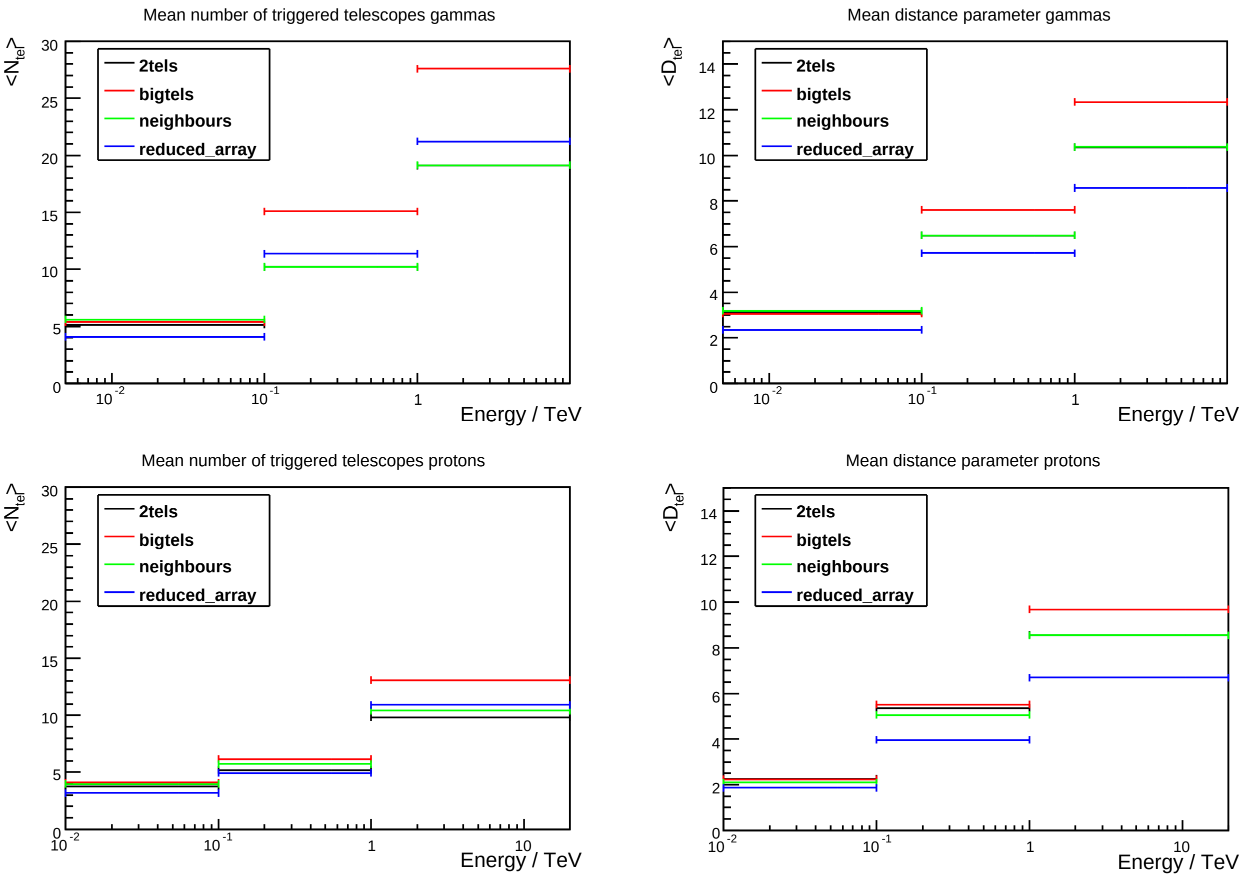

Figure 4.9: Left: Mean values per energy band of the distributions of the number of triggered telescopes for γ rays (above) and for protons (bellow). The mean values are calculated from the curves from figures 4.5, 4.6 respectively.
Right: Mean values per energy band of the distributions of the distance parameter for γ rays (above) and for protons (bellow). The mean values are calculated from the curves from figures 4.7, 4.8 respectively.
The different colors represent different trigger criteria from table 4.1.

The trend is that more cells of the array are triggered as the energies increases because the event lightpool is bigger, as seen in figures 4.7 and 4.8. In this case at high energies the big telescopes (red curve) still make the difference, like for the number of triggered telescopes: they become a better mean value of the distance parameter because of the border minimization effect. But now the blue curve (reduced array) has the lowest values because of the smaller size of the array, which is sometimes saturated as already explained for figures 4.5 and 4.6.

Once again the black (all stereoscopic events) and the green (neighbouring events) points fall together like in the case of the number of triggered telescopes.

And also the differences are smaller in the case of protons, due to their bigger and more irregular lightpools.

To finish with the overview of the simulated data, the mean values for the distributions of all the energies (black curves from figures 4.5, 4.6 and 4.7, 4.8) can be seen in tables 4.3 and 4.4.

	Mean number of triggered telescopes			
particle	2tels	bigtels	neighbours	reduced_array
γ rays	6.69	7.45	7.17	6.55
protons	4.96	5.71	5.36	4.61

Table 4.3: Mean number of triggered telescopes for each trigger criterion. The mean value has been calculated from the black curves (all energies) of figures 4.5 and 4.6.

	Mean distance parameter			
particle	2tels	bigtels	neighbours	reduced_array
γ rays	4.12	4.01	4.26	3.45
protons	4.39	4.40	4.15	3.31

Table 4.4: Mean value of the scaled (50 m) maximum distance between pairs of triggered telescopes (distance parameter) for each trigger criterion. The mean value has been calculated from the black curves (all energies) of figures 4.7 and 4.8.

From the tables it is clear that the γ rays cover ~ 4 cells of the array (200 m) triggering ~ 7 telescopes, whereas the protons trigger less telescopes in mean (~ 5). These values are quite stable for all the trigger criteria, and will be important later on for the data flow estimation.

4.3 TRIGGER RATES

After having looked at the events in more detail, the effective areas and trigger rates for each trigger criterion will be presented in this section.

4.3.1 Spectra

First of all, the used spectra will be presented.

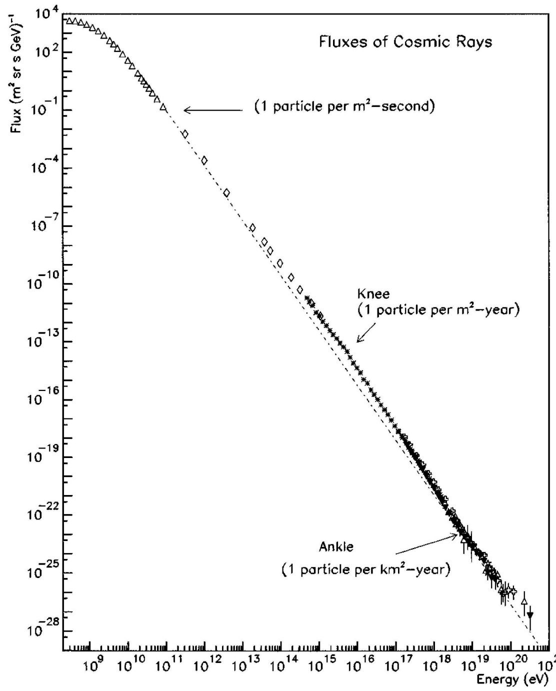

Figure 4.10: Cosmic ray spectrum. Figure taken from [22].

In the first approximation, the cosmic ray spectrum (see figure 4.10) can be described by a simple power-law function:

$$\frac{\mathrm{d}\phi}{\mathrm{d}E} = \phi_0 \left(\frac{E}{E_0}\right)^{-\alpha}$$

where:

- ϕ flux
- E energy
- ϕ_0 flux normalization
- E_0 normalization energy (for the units)
- α spectral index (sometimes also $-\alpha$)

But there can be some deviations, like a change on the exponent, or a cut-off.

For the γ ray data, the Crab Nebula spectrum measured by HESS (see [2]) will be used:

$$\frac{\mathrm{d}\phi}{\mathrm{d}E} = 3.76 \times 10^{-7} \Big(\frac{E}{\mathrm{TeV}}\Big)^{-2.39} \; 1/(\mathrm{s\,m^2\,TeV})$$

In this study the cut-off seen by HESS will be ignored for simplicity: as it is at high energies (where the spectrum is already very low), this will not affect the results.

The reason to use the Crab Nebula is because it is the "standard" source for γ ray astronomy.

The statistical error of the spectrum measurement is a systematic error for the trigger rate calculation. For that reason, the value of 1.9% will be taken as the relative uncertainty in the flux measurement (taken from the paper mentioned above).

For the proton data, there are two possibilities (see figure 4.11 above):

The HEGRA measurement of the cosmic ray flux spectrum (see [1]):

$$\frac{\mathrm{d}\phi}{\mathrm{d}E} = 0.11 \Big(\frac{E}{\mathrm{TeV}}\Big)^{-2.72} \; 1/(\mathrm{s\ sr\,m^2\,TeV})$$

A pure power-law. This was measured from 1.5 TeV to 3 TeV with 18% accuracy.

Or the BESS measurement of the proton flux (see [23]):

$$\frac{\mathrm{d}\phi}{\mathrm{d}E} = 0.099 \, \frac{(E\,[\mathrm{TeV}])^{-2.70}}{1 + (0.004/E\,[\mathrm{TeV}])^{1.75}} \; 1/(\mathrm{s\,sr\,m^2\,TeV})$$

A power-law with a cut-off at low energies at $E = 4$ GeV. This was measured from 1 GeV to 120 GeV with 5% accuracy. (The fit was not published.) The cut-off at low energies is due to the magnetic field of the Earth.

In the same figure but below the relative variation between them is shown:

$$\frac{\left.\frac{\mathrm{d}\phi}{\mathrm{d}E}\right|_{\mathrm{BESS}} - \left.\frac{\mathrm{d}\phi}{\mathrm{d}E}\right|_{\mathrm{HEGRA}}}{< \left.\frac{\mathrm{d}\phi}{\mathrm{d}E}\right|_{\mathrm{BESS}} + \left.\frac{\mathrm{d}\phi}{\mathrm{d}E}\right|_{\mathrm{HEGRA}} >}$$

In the figure it is to see that the differences tend to disappear with growing energies. So the following criterion will be taken: the BESS spectrum will be used with 5% error below 120 GeV and 18% error above 120 GeV.

4.3.2 Effective areas

The effective areas were calculated with the EffectiveAreaMaker, a standard tool from the HESS software. For the γ rays, a point-like source was simulated, but for the protons it was an extended emission, so one has to multiply by the solid

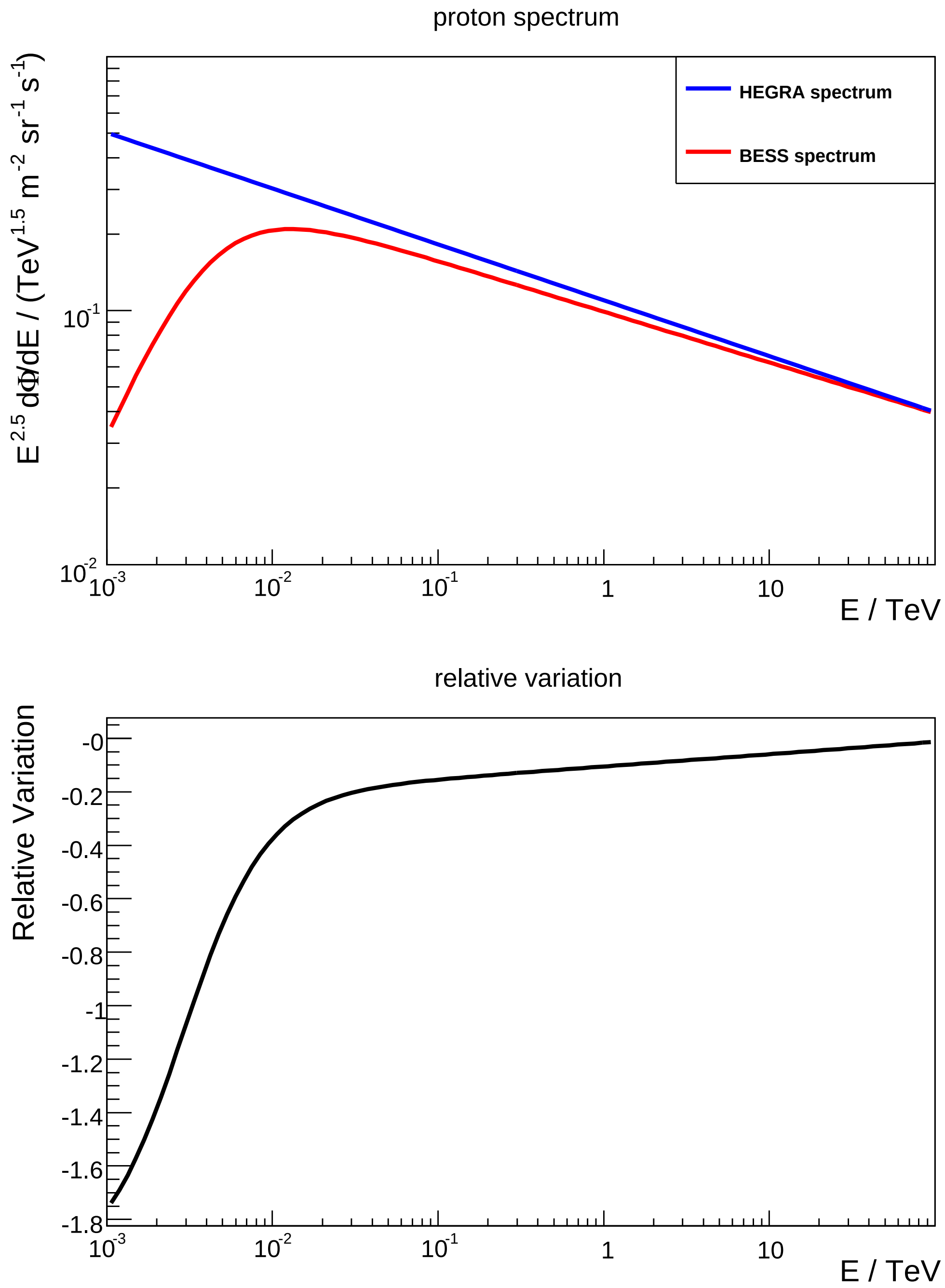

Figure 4.11: Proton spectrum (above): blue for HEGRA (extrapolated for low energies), red for BESS (extrapolated for high energies). The differential flux has been multiplied by $E^{2.5}$ to enhance the difference. In black (below): relative variation between both.

angle within the events were simulated in order to get the trigger rate, since the spectrum has the same dependence, an they thus cancel in the calculation of the rate. The formulas used to calculate the effective areas A_{eff} are:

$$A_{\text{eff}}|_{\gamma}(E) = \pi R^2 \frac{N_{\text{sel}}(E)}{N_{\text{sim}}(E)}$$
$$A_{\text{eff}}|_{\text{proton}}(E) = \pi R^2 \, \Omega \, \frac{N_{\text{sel}}(E)}{N_{\text{sim}}(E)}$$

where:

- R radius within the particles were simulated
- Ω solid angle within the particles were simulated (in case of diffuse emission like protons)
- N_{sim} simulated events
- N_{sel} events passing the trigger condition

The effective areas for both γ rays and protons are shown on the left side of figure 4.12 for each trigger criterion.

The general trend is a steep growth that tends to a saturation value at high energies. The double structure due to the change of curvature is produced by the existence of two kind of telescopes: the big telescopes for the low energies and the small ones for the high energies.

Looking at the trigger criteria, the neighbouring telescope scheme performs quite similar to the criterion where all stereo events are taken (green and black curves respectively), but still has a slightly better background rejection: the effective area for protons is a bit lower, whereas for γ rays it is almost the same. This happens because of the more irregularity in the proton showers: they tend to be more spread out, so asking for neighbouring telescopes rejects more of them. Something similar happens with the big telescopes and the reduced array (red and blue curves respectively) at high energies: they overlap, but the reduced array has a better background rejection. At low energies it is straightforward that the big telescopes have a higher effective area, due to their bigger dishes, but they perform not so well at high energies due to their smaller FOV.

4.3.3 Trigger rates

Assuming the spectra described above, the trigger rate R is calculated as the integral over the energy of the effective area multiplied by the differential flux (flux spectrum):

$$R = \int \mathrm{d}E \, A_{\text{eff}} \, \frac{\mathrm{d}\phi}{\mathrm{d}E}$$

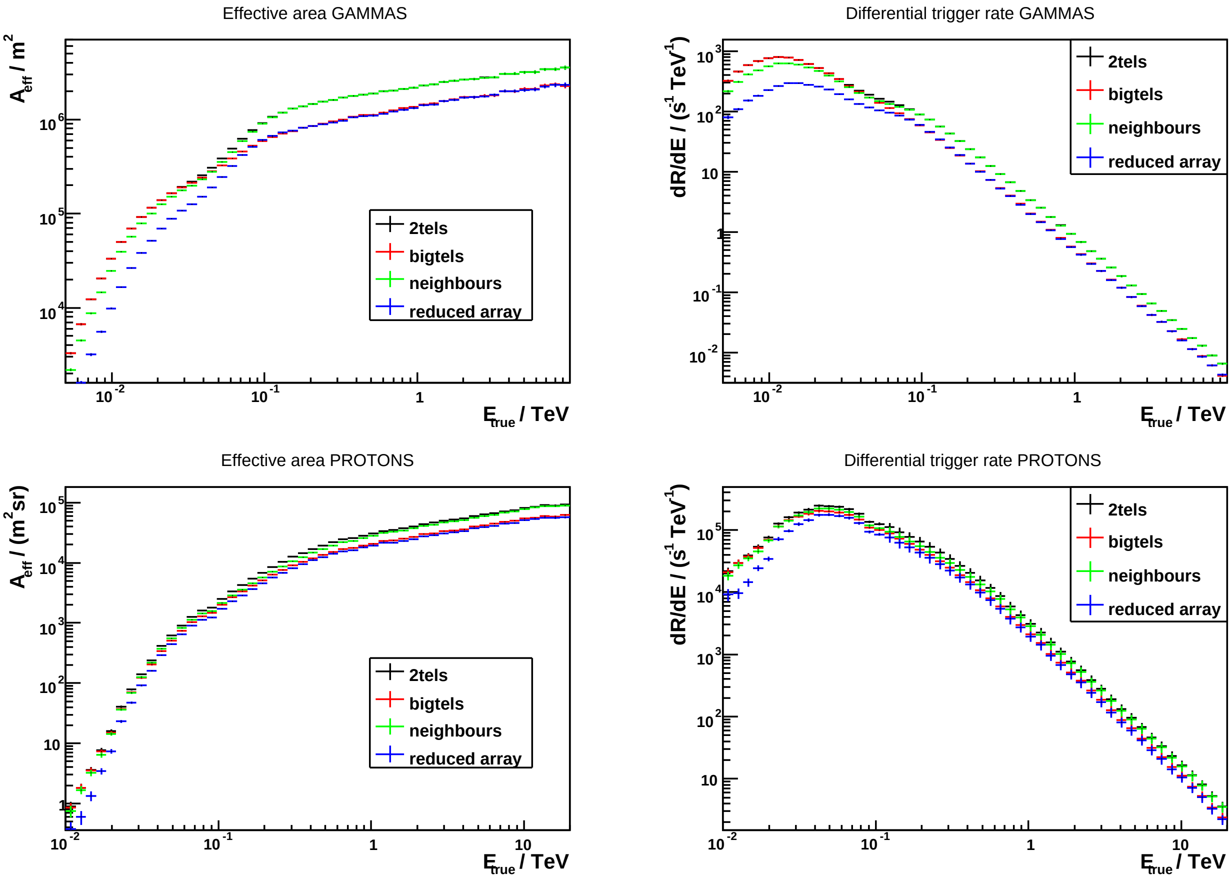

Figure 4.12: Effective areas (left) and differential trigger rates (right) as a function of the simulated energy for γ rays (above) and protons (below). The different colors represent different trigger criteria from table 4.1.

or in the discrete form

$$R = \sum_i \frac{\mathrm{d}R}{\mathrm{d}E}\Big|_i \Delta E_i$$

where

$$\frac{\mathrm{d}R}{\mathrm{d}E} = A_{\mathrm{eff}} \frac{\mathrm{d}\phi}{\mathrm{d}E}$$

is the differential trigger rate.

In a more compact form, one can write: $R = N/T$, where N is the number of triggered events and T is the live time of data taken. This formula was used in the table of subsection 3.2.3 to calculate the equivalent measurement times.

For the error, there are two major contributions: the statistical error in the calculation of the effective areas $\sigma_{A_{\mathrm{eff}}}$, and the relative uncertainty in the spectrum measurement $\varepsilon_{\mathrm{rel}}(\phi_0)$. As they are uncorrelated, the total error is the squared addition of both contributions:

$$\sigma_R = \sqrt{\sum_i \left[\left[\left(\sigma_{A_{\mathrm{eff}}} \frac{\mathrm{d}\phi}{\mathrm{d}E}\Big|_i \right)^2 + \left(\varepsilon_{\mathrm{rel}}(\phi_0) \frac{\mathrm{d}R}{\mathrm{d}E}\Big|_i \right)^2 \right] \Delta E_i^2 \right]}$$

where the error in the effective area is calculated via the variance of the binomial distribution of $\epsilon = N_{\mathrm{sel}}/N_{\mathrm{sim}}$ (see [7]), so in case of γ rays it is:

$$\sigma_{A_{\mathrm{eff}}}(E) = \pi R^2 \sqrt{\frac{\epsilon(1-\epsilon)}{N_{\mathrm{sim}}}}$$

(the same formula multiplied by Ω is used for protons).

The differential trigger rates for both γ rays and protons are shown on the right side of figure 4.12 for each trigger criteria.

The general trend of the curves is a maximum value at low energies, and a potential fall down towards high energies. In these plots, the same double structure is seen as for the effective areas, and also the same remarks done for those plots apply here.

From the differential trigger rate curves it is possible to get the energy threshold and the trigger rate of the system.

The energy threshold E_{th} of a Cherenkov telescope system is usually defined as the energy at the maximum of the differential trigger rate curve for γ rays. The values for each trigger criterion can be seen in table 4.5.

All perform very similar, but one can see that the request that at least one big telescope has triggered produces the lowest threshold.

The actual rates for each trigger criterion are calculated by just integrating the differential trigger rate curves. And since the effective areas have been calculated

Trigger criterion	Rate(γ) / Hz	Rate(p) / Hz	Energy threshold / GeV
2tels	34.27 ± 0.14	$(34.6 \pm 1.1) \times 10^3$	$11.6^{+0.8}_{-0.9}$
bigtels	28.63 ± 0.12	$(26.6 \pm 0.8) \times 10^3$	$11.6^{+0.8}_{-0.9}$
neighbours	31.03 ± 0.12	$(30.3 \pm 0.9) \times 10^3$	$13.4^{+1.1}_{-1.0}$
reduced_array	18.19 ± 0.08	$(23.1 \pm 0.7) \times 10^3$	$15.6^{+1.2}_{-1.1}$

Table 4.5: Calculated trigger rates and energy thresholds for each trigger criteria. For γ rays the HESS Crab Nebula spectrum was used and for protons the BESS spectrum (see subsection 4.3.1). These results complement the ones presented in [21].

at the trigger level, these will be the actual trigger rates one would expect for each configuration. The values can be seen in table 4.5.

Comparing the values between γ rays and protons ($R_{\text{p}}/R_{\gamma} \sim 10^3$) it is clear that the rate is dominated by proton events (background). The aim is to reduce this rate, without loosing too much from the γ ray events.

Looking at the trigger criteria, as it was expected, the biggest rate comes from the "2tels" criterion, where all stereo events are. The second highest value belongs to the neighbouring scheme, which means that almost all the stereo events are compact events, in the sense that they trigger next-to-each-other telescopes. The big telescopes also have a high rate, and the lowest rate comes from the reduced array.

As it was said on subsection 3.1.2, the random trigger due to NSB should be calculated. The formula used for that (see [14]) is the following one:

$$R_{\text{acc, sys}} = M \times \mathcal{C} \times R^{M}_{\text{acc, single}} \times T^{M-1}$$

where

- $R_{\text{acc, sys}}$ is the random rate of the array due to NSB.
- M is the required telescope multiplicity for the trigger system (2 in this case).
- $\mathcal{C}$ is the number of possible combinations of M telescopes out of the whole array (97 telescopes).
- $R_{\text{acc, single}}$ is the random rate of one telescope due to NSB (100 Hz in this case - see subsection 3.2.2).
- T is the allowed time window for coincidence inter telescope trigger.

Some values are shown in table 4.6.

T / ns	$R_{\mathrm{acc,\,sys}}$ / Hz
10	0.93
100	9.3
200	18.6

Table 4.6: Random NSB trigger as a function of the time window allowed for telescope coincidence, with a requirement of at least 2 telescopes and a pixel threshold that allows a maximum of 100 Hz NSB camera trigger.

It is clear that in any case this quantity is very small compared to the ~ 30 kHz from the proton rate, and can be ignored: for the most reasonable value of 100 ns time window it is only a ~ 0.03 % factor. In case of a lower pixel threshold, allowing something like 1 kHz camera trigger due to NSB the rate is not so small: 930 Hz for the case of 100 ns time window, and it should be taken into account (~ 1 kHz $\rightarrow \sim 3\%$ of the proton rate).

With the neighbouring scheme, one requires that next to each other telescopes trigger, so this rate should be very small in that case, even for a high NSB rate, so the pixel threshold could be lower.

4.3.4 Signal to noise ratio

Once the distributions of the differential trigger rates for both γ rays and protons have been calculated, it is possible to calculate the expected signal-to-noise (S/N) ratio by dividing both histograms (where the γ rays are the signal and the protons are the noise), taking into account that the background for 1 TeV γ rays is produced by protons with $E \simeq 3$ TeV.

This happens because a proton of energy $3E$ produces approximately so much light in the telescopes as a proton of energy E. The reason is that the protons in the atmosphere undergo in the first collision via strong interaction, producing some other hadrons (for which the process is recursive) and mesons, mostly pions: π^+, π^0, π^- with probability $\sim 1/3$ for each kind of decay. As only the π^0 decays electromagnetically:

$$\pi^0 \rightarrow \gamma\gamma$$

only $1/3$ of the energy will undergo in electromagnetic showers and therefore the telescopes are only sensitive to $1/3$ of the energy. (See [24] for example.)

If the reconstruction method uses energy lookups done for γ rays for both γ rays and protons (as it is the case for the HESS software), one can write:

$$E_{\mathrm{reco}}(\gamma) \simeq E_{\mathrm{true}}(\gamma)$$

$$E_{\mathrm{reco}}(\mathrm{proton}) \simeq \frac{1}{3} E_{\mathrm{true}}(\mathrm{proton})$$

where

- E_{true} is the simulated energy.
- E_{reco} is the reconstructed energy: the energy measured by the telescope.

Taking this into account and therefore scaling the proton energy by 1/3 (since the dependency is on the true energy) , the S/N ratio can be calculated with the formula:

$$S/N(E) = \frac{\left.\frac{\mathrm{d}R}{\mathrm{d}E}\right|_{\gamma}(E)}{\left.\frac{\mathrm{d}R}{\mathrm{d}E}\right|_{\text{proton}}(3E)}$$

The S/N ratio for each trigger criterion is shown in figure 4.13.

The trend of all the curves is a more or less linear growth, which means a better ratio with growing energies. This is explained by the different indexes of the spectra: protons have a steeper spectra than the γ rays (index 2.70 and 2.39 respectively), so the signal to noise ratio increases with the energy. There is also a small peak at low energies, due to the double structure already discussed for the effective areas plots.

Comparing the trigger criteria, all schemes perform very similar. However, taking into account figure 4.12 the big telescopes trigger at low energies much more γ rays than the other trigger schemes, but in comparison not much more protons, so they have the best rejection at low energies. At high energies it is just the opposite, so they have the worst ratio above 100 GeV. It is also remarkable, that the best ratio at high energies comes from the neighbouring scheme (green curve), which has a better proton rejection than the criterion where all stereoscopic events are kept.

The reduced array (blue curve) presents the worst ratio at low energies. The reason for that is that the ratio of big to small telescopes is smaller for the reduced array than for the whole array: there are relatively less big telescopes, so the ratio is worse for the low energy range. At high energies the ratio is also not so good as for the neighbouring scheme because of the smaller area of the array.

The effect of the big telescopes can also be noticed at the trigger rates (figure 4.12 and table 4.5): the differential trigger rate at low energies is significantly worse for γ rays than it is for protons for the reduced array compared to the whole array, meaning that the big telescopes are really important at low energies, and also at the overall trigger rate, making the rate of the reduced array the lowest one. The difference is not so big for protons because of their bigger and more irregular lightpools, which make them trigger the array with a higher probability: this effect can be seen at figures 4.2 and 4.3, where the γ rays are more localized

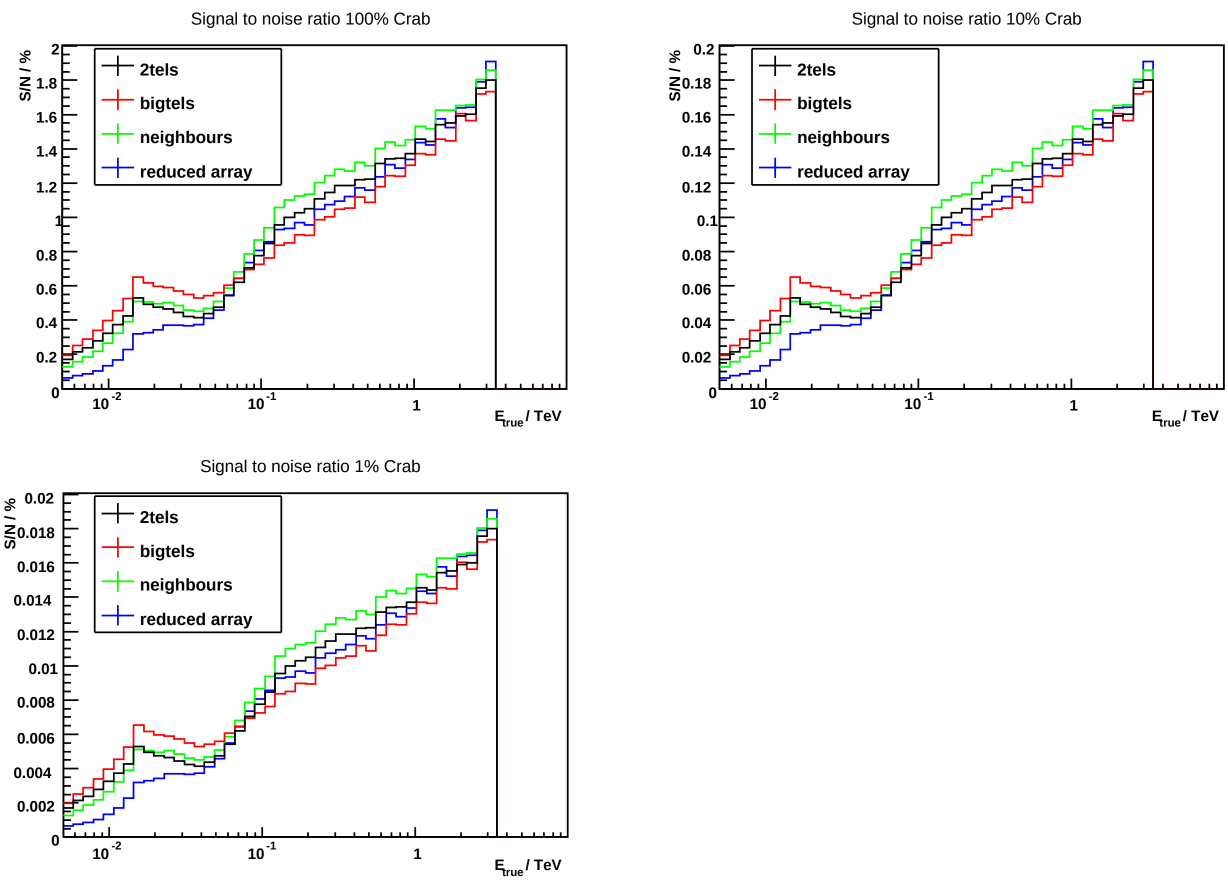

Figure 4.13: Signal to noise ratio for different percentages of the Crab Nebula flux: 100%, 10% and 1% (indicated in the title of each plot). The percentages were applied to the normalization factor of the Crab Nebula flux spectrum, not to the integral. The different colors represent the different trigger criteria from table 4.1.

within the array than the protons (one can also see, that the proton map almost remains the same for all the trigger criteria).

Chapter 5

Conclusions and outlook

Referring to what was said in the introduction, it seems that CTA will consist of a $\mathcal{O}(50)$ telescope array. Taking this into account, the here analyzed array of 97 telescopes is not the most realistic one, but still it is useful in order to develop and test the triggering tools which later on will be used for the preliminary arrays in order to develop the triggering techniques for CTA.

Having said that, the most realistic trigger criterion from the ones presented here, is the neighbouring scheme. Even though the performance in the study presented here is not the best one (that was not the aim of this work, since it is the first of many studies referred to the trigger), it is the most flexible one: this method is not meant to be exclusive, but it could be combined with other ones. For example, for a low energy source, one could request a neighbouring trigger applied for events triggering the big telescopes. It could also be possible to go further and request more than two neighbouring telescopes or even make a double system in which one asks not only for neighbouring telescopes, but for neighbouring islands (or telescope clusters), or even a certain amount of neighbouring islands. In this way, it could be interesting to look into patterns on the triggered telescopes and maybe achieve like this some degree of hadron rejection, since their showers are much more irregular than for protons (at least at high energies).

This neighbouring scheme takes almost all the stereo events and rejects more background, having a better S/N ratio at high energies and a better rejection of NSB random triggers. For this trigger scheme, the expected data transfer rate can be estimated with the results from the analysis in section 4 and the estimation from the CTA-ELEC-WP (the electronics working package, which is responsible of the design of the trigger system for CTA, among other subtasks) of how much information per channel should be saved. With an estimation of $\sim$ 30 Bytes/pixel for an event (if timing information is saved - see [14]), roughly $\sim$ 3000 pixels/camera (see subsection 3.2.1) and a mean number of $\sim$ 5 triggered telescopes per proton event (see 4.3), the expectation is 440 kB/event, which means, considering the trigger rate of $\sim$ 30 kHz (see 4.5), a data transfer rate of $\sim$ 13 GB/s. For γ ray events, there are more triggered telescopes in mean (7, see 4.3) so the expectation is 615 kB/event, but, since the trigger rate is much smaller, the effect to the data flow is negligible, so it will not be taken into account for the following numbers.

For events without timing information, the estimation is $\sim$ 3 Bytes/channel (a factor 10 less disk space), so the rate would be $\sim$ 1.3 GB/s. The LHC does full offline event reconstruction at a rate of $\sim$ 1 GB/s, so for CTA ($\sim$ 2015) with the expected technological development, it should be possible to do almost full event reconstruction with a moderate size farm, and sort out the most obvious hadronic showers, gaining a factor 10 in background suppression.

With timing information, the data rate is again $\sim$ 13 GB/s, so maybe the event reconstruction is not the best idea, and one should do the rejection before. A possibility could be to send only a part of the information from the camera (the parametrization - Hillas parameters - from the image):

$$100\,\text{bytes/image} \times 5\,\text{cameras/event} \times 30\,\text{kHz} = 14\,\text{MB/s}$$

This should be fast enough within the camera possibilities (1 or 2 seconds buffer storing capabilities - see [14]) in order to do a fast event reconstruction and discard the most obvious hadrons by a factor of 10, reducing the rate to $\sim$ 1.3 GB/s and continue as mentioned above.

Anyway, these numbers should be taken as orientation values, and not definitive, since the simulated data used here is not complete: the energy range should be extended, as well as the simulation radius for the protons, and the simulation of the NSB should be corrected. Plus, the $L1$ trigger scheme may change.

To conclude, as already mentioned in this work, the simulated array is not the definitive one, and also the trigger scheme should be further developed, so this analysis will be repeated and some other new ones will be performed after the first mass production of Monte Carlo data for CTA in the autumn of 2008.

Bibliography

[1] F. Aharonian, A. G. Akhperjanian, J. A. Barrio, A. S. Belgarian, K. Bernlöhr, J. J. Beteta, H. Bojahr, S. Bradbury, I. Calle, J. L. Contreras, J. Cortina, A. Daum, T. Deckers, S. Denninghoff, V. Fonseca, J. C. Gonzalez, G. Heinzelmann, M. Hemberger, G. Hermann, M. Hess, A. Heusler, W. Hofmann, H. Hohl, I. Holl, D. Horns, A. Ibarra, R. Kankanyan, M. Kestel, O. Kirstein, C. Köhler, A. Konopelko, H. Kornmeyer, D. Kranich, H. Krawczynski, H. Lampeitl, A. Lindner, E. Lorenz, N. Magnussen, H. Meyer, R. Mirzoyan, A. Moralejo, L. Padilla, M. Panter, D. Petry, R. Plaga, A. Plyasheshnikov, J. Prahl, C. Prosch, G. Pühlhofer, G. Rauterberg, C. Renault, W. Rhode, A. Röhring, V. Sahakian, M. Samorski, D. Schmele, F. Schröder, W. Stamm, H. J. Völk, B. Wiebel-Sooth, C. A. Wiedner, M. Willmer, and H. Wirth. Cosmic ray proton spectrum determined with the imaging atmospheric Cherenkov technique. *Physical Review D (Particles and Fields), Volume 59, Issue 9*, 1999.

[2] F. Aharonian, A. G. Akhperjanian, A. R. Bazer-Bachi, M. Beilicke, W. Benbow, D. Berge, K. Bernlöhr, C. Boisson, O. Bolz, V. Borrel, I. Braun, F. Breitling, A. M. Brown, R. Bühler, I. Büsching, S. Carrigan, P. M. Chadwick, L.-M. Chounet, R. Cornils, L. Costamante, B. Degrange, H. J. Dickinson, A. Djannati-Ataï, L. O'C. Drury, G. Dubus, K. Egberts, D. Emmanoulopoulos, P. Espigat, F. Feinstein, E. Ferrero, A. Fiasson, G. Fontaine, S. Funk, S. Funk, Y. A. Gallant, B. Giebels, J. F. Glicenstein, P. Goret, C. Hadjichristidis, D. Hauser, M. Hauser, G. Heinzelmann, G. Henri, G. Hermann, J. A. Hinton, W. Hofmann, M. Holleran, D. Horns, A. Jacholkowska, O. C. de Jager, B. Khélifi, N. Komin, A. Konopelko, K. Kosack, I. J. Latham, R. Le Gallou, A. Lemière, M. Lemoine-Goumard, T. Lohse, J. M. Martin, O. Martineau-Huynh, A. Marcowith, C. Masterson, T. J. L. McComb, M. de Naurois, D. Nedbal, S. J. Nolan, A. Noutsos, K. J. Orford, J. L. Osborne, M. Ouchrif, M. Panter, G. Pelletier, S. Pita, G. Pühlhofer, M. Punch, B. C. Raubenheimer, M. Raue, S. M. Rayner, A. Reimer, O. Reimer, J. Ripken, L. Rob, L. Rolland, G. Rowell, V. Sahakian, L. Saugé, S. Schlenker, R. Schlickeiser, U. Schwanke, H. Sol, D. Spangler, F. Spanier, R. Steenkamp,

C. Stegmann, G. Superina, J.-P. Tavernet, R. Terrier, C. G. Théoret, M. Tluczykont, C. van Eldik, G. Vasileiadis, C. Venter, P. Vincent, H. J. Völk, S. J. Wagner, and M. Ward. Observations of the Crab nebula with HESS. *Astronomy and Astrophysics, Volume 457, Issue 3, October III 2006, pp.899-915*, 2006.

[3] D. Berge, S. Funk, and J. Hinton. Background modelling in very-high-energy γ-ray astronomy. *Astronomy and Astrophysics, Volume 466, Issue 3, May II 2007, pp.1219-1229*, 2006.

[4] K. Bernlöhr. Performance details of Heidelberg array configurations. *CTA-MC-WP meeting talk*, 2008.

[5] K. Bernlöhr. Simulation of imaging atmospheric Cherenkov telescopes with CORSIKA and sim_telarray. *Astroparticle Physics*, 2008.

[6] K. Bernlöhr et. al. MC Simulation and Layout Studies for a future Cherenkov Telescope Array. *30th International Cosmic Ray Conference (ICRC)*, 2007.

[7] V. Blobel and E. Lohrmann. Statistische und numerische Methoden der Datenanalyse. *B.G. Teubner Stuttgart-Leipzig*, 1998.

[8] G. Cabras, A. de Angelis, B. de Lotto, M. M. de Maria, F. de Sabata, O. Mansutti, M. Frailis, M. Persic, C. Bigongiari, M. Doro, M. Mariotti, L. Peruzzo, A. Saggion, V. Scalzotto, R. Paoletti, A. Scribano, N. Turini, A. Moralejo, and D. Tescaro. A novel background reduction strategy for high level triggers and processing in gamma-ray Cherenkov detectors. *FRONTIERS OF FUNDAMENTAL AND COMPUTATIONAL PHYSICS: 9th International Symposium. AIP Conference Proceedings, Volume 1018, pp. 180-183*, 2008.

[9] J. Cortina. Status and First Results of the Magic Telescope. *Astrophysics and Space Science, Volume 297, Issue 1-4, pp. 245-255*, 2005.

[10] CTA Consortium. www.cta-observatory.org.

[11] S. Ehlert. HESS Phase II Performance Characteristics: The First Analysis. *HESS internal talk*, 2008.

[12] S. Funk, G. Hermann, J. Hinton, D. Berge, K. Bernlöhr, W. Hofmann, P. Nayman, F. Toussenel, and P. Vincent. The trigger system of the H.E.S.S. telescope array. *Astroparticle Physics, Volume 22, Issue 3-4, p. 285-296*, 2004.

[13] P. Goret et. al. SAM (Swift Analogue Memory): a new GHz sampling ASIC for the HESS-II FEE. *Proc. Conf. Towards a Network of Atmospheric Cherenkov Detectors VII*, 2005.

[14] G. Hermann. CTA. Some thoughts about the System Trigger. *CTA-ELEC-WP meeting talk*, 2008.

[15] G. Hermann, W. Hofmann, T. Schweizer, M. Teshima, and f. t. CTA consortium. Cherenkov Telescope Array: The next-generation ground-based gamma-ray observatory. *30th International Cosmic Ray Conference (ICRC)*, 2007.

[16] H.E.S.S. collaboration. The H.E.S.S. Software User Manual. *HESS internal note (unpublished)*, 2003.

[17] K. Kosack. HESS Analysis. *CTA-DATA-WP meeting talk*, 2008.

[18] K. Kosack. HAP Overview Status. *HESS collaboration meeting talk*, 2008.

[19] K. Kosack et. al. HAP Tutorial. *HESS internal web pages (unpublished)*, 2008.

[20] M. Paz Arribas. HESS II studies with HAP. *HESS collaboration meeting talk*, 2008.

[21] M. Paz Arribas. CTA trigger studies with HAP. *CTA-MC-WP meeting talk*, 2008.

[22] D. Perkins. Particle Astrophysics. *Oxford University Press*, 2005.

[23] T. Sanuki, M. Motoki, H. Matsumoto, E. S. Seo, J. Z. Wang, K. Abe, K. Anraku, Y. Asaoka, M. Fujikawa, M. Imori, T. Maeno, Y. Makida, N. Matsui, H. Matsunaga, J. Mitchell, T. Mitsui, A. Moiseev, J. Nishimura, M. Nozaki, S. Orito, J. Ormes, T. Saeki, M. Sasaki, Y. Shikaze, T. Sonoda, R. Streitmatter, J. Suzuki, K. Tanaka, I. Ueda, N. Yajima, T. Yamagami, A. Yamamoto, T. Yoshida, and K. Yoshimura. Precise Measurement of Cosmic-Ray Proton and Helium Spectra with the BESS Spectrometer. *The Astrophysical Journal, Volume 545, Issue 2, pp. 1135-1142*, 2000.

[24] S. Schlenker. Simulation Study for the H.E.S.S. Single Telescope Trigger Rate. *Humboldt University diploma thesis*, 2001.

[25] F. Schmidt. Search for pulsed TeV Gamma-Ray Emission from Pulsars with H.E.S.S. *Humboldt University diploma thesis*, 2005.

[26] U. Schwanke. Data Acquisition and Computing at H.E.S.S. *DESY Computing Seminar talk*, 2006.